Pergamon

Int. J. Heat Mass Transfer. Vol. 40, No. 4, pp. 893–903, 1997

0017-9310/97 $17.00+0.00

PII: S0017-9310(96)00157-3

A numerical study of unsteady free convection from a sphere in a porous medium

B. YAN
School of Mathematics, University of East Anglia, Norwich NR4 7TJ, U.K.

I. POP
Faculty of Mathematics, University of Cluj, R-3400 Cluj, Romania

and

D. B. INGHAM
Department of Applied Mathematical Studies, University of Leeds, Leeds LS2 9JT, U.K.

(*Received* 16 *April* 1996)

Abstract—In this paper a transient free convection flow from a sphere which is embedded in a porous medium has been considered. The temperature or heat flux of the sphere is suddenly raised and subsequently maintained at constant values over the surface. The coupled governing equations of the Darcy flow and energy are solved numerically for both small and large values of the Rayleigh number using a classical finite-difference method. Transient and steady-state flow and temperature patterns around the sphere are discussed in detail and a comparison of the overall Nusselt number with some earlier results shows very good agreement. Copyright © 1996 Elsevier Science Ltd.

1. INTRODUCTION

Buoyancy-driven flows in fluid-saturated porous media occur in many practical applications and have been studied extensively during the last three decades. Nield and Bejan [1] and Nakayama [2] cite a number of specific examples ranging from natural processes to those of technological importance. Recently, the technical interest in convective heat transfer in porous media has exploded and this is probably due to its wide range of applications in contemporary technologies, such areas as the thermal insulation of buildings, nuclear energy systems, the storage of grain, fruits and vegetables, in petroleum reservoirs and catalytic reactors.

Studies of flows associated with a body embedded in fluid-saturated porous media have mainly been concentrated on flat plates, cylinders and spheres. Yamamoto [3] was the first to consider the problem of steady natural convection around an isothermal sphere in a porous medium. He obtained series solutions for $Ra \ll 1$, where Ra is a suitably defined Rayleigh number. Subsequently, Merkin [4] and Nakayama and Koyama [5] considered the flow in the limiting case of $Ra \to \infty$, i.e. boundary-layer approximation, whilst Pop and Ingham [6] studied both the cases of small and large values of Ra using a finite-difference scheme for an isothermal sphere.

However, very little work has been performed for the problem of unsteady free convection from a sphere which is embedded in a porous medium and, to our knowledge, there are only three recent papers on this problem. Sano and Okihara [7] have studied the transient case using asymptotic solutions in terms of small Ra, Nguyen and Paik [8] have investigated numerically the unsteady mixed convection from a sphere in a porous medium saturated with water using a Chebyshev–Legeure spectral method, whilst Miloh and Tyvand [9] have analysed the development of the initial free convection around an isothermal sphere in a porous medium by the method of matched asymptotic expansions. The Rayleigh number Ra is assumed to be large, but finite, and the solution is only obtained for small values of time.

The present study is carried out to investigate the transient nature of free convection associated with a sphere which is embedded in a fluid-saturated porous medium and whose surface is impulsively changed to a constant temperature or constant heat flux. The Rayleigh number is assumed to be finite so that no simplifying assumptions, other than the Darcy–Boussinesq approximation, are made in the coupled momentum and energy equations. These equations are properly transformed and solved using a method similar to that proposed by Riley [10]. The calculations are extended to a sufficiently large time such

NOMENCLATURE

a	radius of the sphere
g	acceleration due to gravity
k	effective thermal conductivity of the fluid-saturated porous medium
K	permeability
Nu	overall Nusselt number defined in equation (24)
q	heat flux
Q	overall heat transfer
r	non-dimensional radial coordinate
Ra	modified Rayleigh number
t	non-dimensional time defined in equation (5)
T	non-dimensional fluid temperature defined in equation (5)
u	non-dimensional velocity in the r direction defined in equation (5)
U_0	characteristic velocity defined in equation (5)
v	non-dimensional velocity in the θ direction defined in equation (5)
x	variable defined in equation (6).

Greek symbols

α	constant introduced in equation (6)
α_m	effective thermal diffusivity of the fluid-saturated porous medium
β	thermal expansion coefficient
δ	mesh size
ΔT	characteristic temperature
ε	prescribed tolerance
η	variable defined as $\eta = x/t^{1/2}$
θ	angular coordinate
μ	variable introduced in equation (6)
ν	kinematic viscosity
σ	ratio of composite material heat capacity to convective fluid heat capacity
ϕ	azimuthal coordinate
ψ	non-dimensional stream function defined in equation (1).

Superscripts

$\bar{}$	dimensional variables
$'$	differentiation with respect to η
m	iteration order.

Subscripts

w	wall condition
∞	ambient condition.

that in the neighbourhood of the sphere the conditions are essentially steady and we are able to compare the results with those predicted by the boundary-layer theory of Pop and Ingham [6] for $Ra \gg 1$.

2. GOVERNING EQUATIONS

Consider a sphere of radius a, which is immersed in a fluid-saturated porous medium which is at a constant temperature T_∞. Suppose that initially the sphere has the same temperature as the porous medium and, at time $\bar{t} = 0$, it is suddenly heated and subsequently maintained (i) at a constant temperature $T_w (> T_\infty)$, or (ii) at a constant heat flux q_w.

A spherical polar coordinate system $(\bar{r}, \theta, \phi)$, with the origin at the centre of the sphere, is chosen with $\theta = 0$ vertically upwards, as shown in Fig. 1. Both the flow and temperature are assumed to be axially symmetrical and hence independent of the azimuthal coordinate ϕ. The fluid motion is described by radial and transversal velocity components $(\bar{u}, \bar{v})$ in a plane through the axis of symmetry. The velocity components are expressed in terms of a dimensionless stream function $\psi(r, \theta)$ by the equations

$$u = \frac{1}{r^2 \sin\theta} \frac{\partial \psi}{\partial \theta} \quad v = -\frac{1}{r \sin\theta} \frac{\partial \psi}{\partial r}. \tag{1}$$

If the physical properties of the fluid are assumed constant and the Darcy–Boussinesq approximation holds, then the non-dimensional governing equations

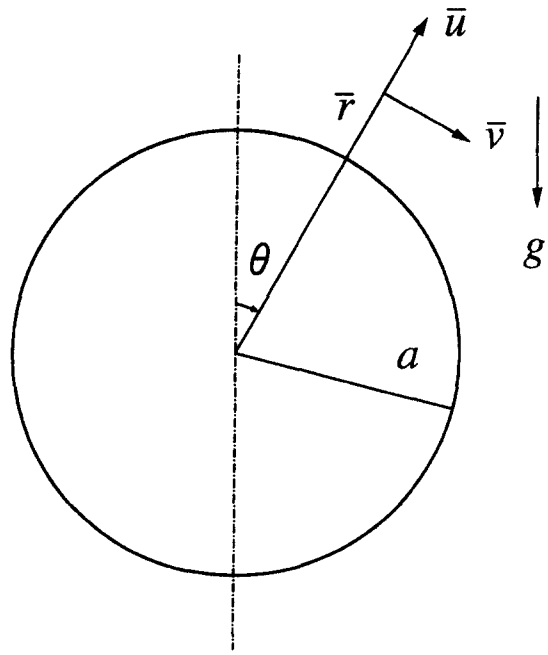

Fig. 1. Physical model and coordinate system.

in terms of the stream function ψ and temperature T can be written as

$$\nabla_1^2\psi = r\sin\theta\left\{\sin\theta\frac{\partial T}{\partial r}+\frac{\cos\theta}{r}\frac{\partial T}{\partial\theta}\right\} \tag{2}$$

$$\frac{\partial T}{\partial t}+\frac{1}{r^2\sin\theta}\left\{\frac{\partial\psi}{\partial\theta}\frac{\partial T}{\partial r}-\frac{\partial\psi}{\partial r}\frac{\partial T}{\partial\theta}\right\} = \frac{1}{Ra}\left[\nabla_1^2 T+\frac{2}{r}\left\{\frac{\partial T}{\partial r}+\frac{\cot\theta}{r}\frac{\partial T}{\partial\theta}\right\}\right] \tag{3}$$

where

$$\nabla_1^2 = \frac{\partial^2}{\partial r^2}+\frac{1}{r^2}\frac{\partial^2}{\partial\theta^2}-\frac{\cot\theta}{r^2}\frac{\partial}{\partial\theta}. \tag{4}$$

The dimensionless variables are defined as

$$\begin{cases} t = U_0\bar{t}/(a\sigma) \quad r = \bar{r}/a \quad u = \bar{u}/U_0, v = \bar{v}/U_0 \\ \text{case (i) } T = (\bar{T}-T_\infty)/\Delta T \quad U_0 = gK\beta\Delta T/\nu \\ \text{case (ii) } T = (\bar{T}-T_\infty)/(q_w a/k) \quad U_0 = gK\beta q_w a/(k\nu) \end{cases} \tag{5}$$

where k is the effective thermal conductivity of the fluid-saturated porous medium, K the permeability of the porous medium, β the coefficient of thermal expansion, σ the ratio of the composite material heat capacity to the convective fluid heat capacity, ν the kinematic viscosity of the fluid, g the acceleration due to gravity, U_0 the characteristic velocity, $\Delta T = T_w - T_\infty$, $Ra = U_0 a/\alpha_m$ the modified Rayleigh number and α_m the effective thermal diffusivity of the fluid-saturated porous medium.

Since the flow experiences larger gradients near the surface of the sphere and in particular near its upper pole similar to that described by Riley [10], we introduce the following transformation:

$$r = \frac{\alpha}{1-x}-\alpha+1 \quad \theta = 2\sin^{-1}\mu \tag{6}$$

where α is a constant which, to some extent, can be used to control the mesh density distribution when we set up the finite-difference scheme. Equations (2) and (3) become, in terms of the new variables (x, μ),

$$\nabla_2^2\psi = 4\alpha\mu^2\frac{1-\mu^2}{1-x}\left\{[(\alpha-1)x+1]\frac{\partial T}{\partial x}+\frac{\alpha(1-2\mu^2)}{4\mu(1-x)}\frac{\partial T}{\partial\mu}\right\} \tag{7}$$

$$\frac{\alpha^2}{(1-x)^2}\frac{\partial T}{\partial t}+\frac{\alpha(1-x)^2}{4[(\alpha-1)x+1]^2\mu}\times\left\{\frac{\partial\psi}{\partial\mu}\frac{\partial T}{\partial x}-\frac{\partial\psi}{\partial x}\frac{\partial T}{\partial\mu}\right\} = \frac{1}{Ra}\left[\nabla_2^2 T+\frac{2\alpha(1-x)}{(\alpha-1)x+1}\times\left\{\frac{\partial T}{\partial x}+\frac{\alpha(1-2\mu^2)}{4\mu(1-x)[(\alpha-1)x+1]}\frac{\partial T}{\partial\mu}\right\}\right] \tag{8}$$

respectively, where

$$\nabla_2^2 = (1-x)^2\frac{\partial^2}{\partial x^2}-2(1-x)\frac{\partial}{\partial x}+\frac{\alpha^2(1-\mu^2)}{4[(\alpha-1)x+1]^2}\left\{\frac{\partial^2}{\partial\mu^2}-\frac{1}{\mu}\frac{\partial}{\partial\mu}\right\}. \tag{9}$$

At $t = 0$, the sphere is heated to a higher temperature than the surrounding fluid, so that the heat transfer is dominated by diffusion in the initial stages until the convection is comparable with the diffusion. It is likely at this early stage that the thickness of the heated layer near the surface is proportional to $t^{1/2}$ and therefore during the initial stages we introduce the variables (η, μ), where $\eta = x/t^{1/2}$. In terms of these new variables, equations (7) and (8) are transformed to

$$\nabla_3^2\psi = 4\mu^2\frac{\alpha(1-\mu^2)}{1-\eta t^{1/2}}\left\{\frac{(\alpha-1)\eta t^{1/2}+1}{t^{1/2}}\frac{\partial T}{\partial\eta}+\frac{\alpha(1-2\mu^2)}{4\mu(1-\eta t^{1/2})}\frac{\partial T}{\partial\mu}\right\} \tag{10}$$

$$\frac{\alpha^2}{(1-\eta t^{1/2})^2}\left\{\frac{\partial T}{\partial t}-\frac{\eta}{2t}\frac{\partial T}{\partial\eta}\right\}+\frac{\alpha(1-\eta t^{1/2})^2}{4\mu t^{1/2}[(\alpha-1)\eta t^{1/2}+1]^2}\times\left\{\frac{\partial\psi}{\partial\mu}\frac{\partial T}{\partial\eta}-\frac{\partial\psi}{\partial\eta}\frac{\partial T}{\partial\mu}\right\} = \frac{1}{Ra}\times\left[\nabla_3^2 T+\frac{2\alpha(1-\eta t^{1/2})}{(\alpha-1)\eta t^{1/2}+1}\left\{\frac{1}{t^{1/2}}\frac{\partial T}{\partial\eta}+\frac{\alpha(1-2\mu^2)}{4[(\alpha-1)\eta t^{1/2}+1]\mu(1-\eta t^{1/2})}\frac{\partial T}{\partial\mu}\right\}\right] \tag{11}$$

respectively, where

$$\nabla_3^2 = \frac{(1-\eta t^{1/2})^2}{t}\frac{\partial^2}{\partial\eta^2}-\frac{2(1-\eta t^{1/2})}{t^{1/2}}\frac{\partial}{\partial\eta}+\frac{\alpha^2(1-\mu^2)}{4[(\alpha-1)\eta t^{1/2}+1]^2}\left\{\frac{\partial^2}{\partial\mu^2}-\frac{1}{\mu}\frac{\partial}{\partial\mu}\right\}. \tag{12}$$

At the initial instant, $t \leqslant 0$, we require

$$\psi = T = 0, \quad \eta > 0, \quad 0 \leqslant \mu \leqslant 1. \tag{13}$$

For $t > 0$, we have for the constant temperature case (i), namely

$$\psi = 0, \quad T = 1, \quad x = 0(\eta = 0) \tag{14}$$

and for the constant heat flux case (ii)

$$\psi = 0, \quad \frac{\partial T}{\partial r} = -1\left(\frac{\partial T}{\partial x} = -\alpha, \frac{\partial T}{\partial\eta} = -\alpha t^{1/2}\right), \quad x = 0(\eta = 0) \tag{15}$$

and at $r = \infty$, which corresponds to $x = 1$, for both cases we set

$$T = \frac{\partial \psi}{\partial x}\left(= \frac{\partial \psi}{\partial \eta}\right) = 0, \quad x = 1, \quad (\eta = t^{-1/2}). \quad (16)$$

Finally, the symmetrical boundary conditions are

$$\psi = 0, \quad \mu = 0,1, \quad 0 \leqslant x \leqslant 1 (0 \leqslant \eta \leqslant t^{-1/2}) \quad (17)$$

and

$$\frac{\partial T}{\partial \mu} = 0, \quad \mu = 0, \quad 0 \leqslant x \leqslant 1 (0 \leqslant \eta \leqslant t^{-1/2}). \quad (18)$$

The corresponding boundary conditions for T at $\mu = 1$ are not so obvious and we will return to this point in the next section.

The solution of equations (10) and (11) in case (i) can be expanded for small values of t and may, to leading order, be expressed as

$$\psi = 4t^{1/2}\mu^2(1-\mu^2)f_0(\eta), \quad T = T_0(\eta) \quad (19)$$

where f_0 and T_0 satisfy the equations

$$f_0''' = \alpha T_0' \quad 2T_0'' + \alpha^2 Ra \eta T_0' = 0 \quad (20)$$

which have to be solved subject to the boundary conditions

$$f_0(0) = 0, \quad T_0(0) = 1, \quad f_0'(\infty) = 0, \quad T_0(\infty) = 0 \quad (21)$$

where primes denote differentiation with respect to η.

The solution of equations (20), subject to boundary conditions (21), can be expressed as

$$\begin{cases} f_0(\eta) = \alpha\eta \operatorname{erfc}(\alpha Ra^{1/2}\eta/2) \\ \qquad + \dfrac{2}{\sqrt{Ra\pi}}(1-\exp(-\alpha^2 Ra\eta^2/4)) \\ T_0(\eta) = \operatorname{erfc}(\alpha Ra^{1/2}\eta/2) \end{cases} \quad (22)$$

where erfc( ) is the complementary error function.

Finally, the overall heat transfer from the sphere can be calculated as,

$$Q = -2\pi ak\,\Delta T \int_0^{\pi} \left.\frac{\partial T}{\partial r}\right|_{r=1} \sin\theta \,\mathrm{d}\theta \quad (23)$$

and therefore the overall Nusselt number is given by

$$Nu = -2\pi \int_0^{\pi} \left.\frac{\partial T}{\partial r}\right|_{r=1} \sin\theta \,\mathrm{d}\theta \quad (24)$$

where $Nu = Q/ka\,\Delta T$. From equation (22), expression (24) becomes

$$Nu \sim 4(\pi Ra/t)^{1/2} \quad (25)$$

for small values of t.

The solution of equations (10) and (11) in case (ii) can also be expanded for small values of t and may, to leading order, be expressed as

$$\psi = 4t\mu^2(1-\mu^2)\tilde{f}_0(\eta), \quad T = \alpha t^{1/2}\tilde{T}_0(\eta) \quad (26)$$

where $\tilde{f}_0$ and $\tilde{T}_0$ satisfy the equations

$$\tilde{f}_0''' = \alpha^2 \tilde{T}_0', \quad 2T_0'' + \alpha^2 Ra(\eta \tilde{T}_0' - \tilde{T}_0) = 0 \quad (27)$$

which have to be solved subject to the boundary conditions

$$\tilde{f}_0(0) = 0, \quad \tilde{T}_0'(0) = -1, \quad \tilde{f}_0'(\infty) = 0, \quad \tilde{T}_0(\infty) = 0. \quad (28)$$

The solution of equations (27), subject to boundary conditions (28), can be expressed as

$$\begin{cases} \tilde{f}_0(\eta) = -\left(\dfrac{1}{Ra} + \dfrac{\alpha^2\eta^2}{2}\right)\operatorname{erfc}(\alpha Ra^{1/2}\eta/2) \\ \qquad + \dfrac{\alpha}{\sqrt{Ra\pi}}\eta \exp(-\alpha^2 Ra\eta^2/4) + \dfrac{1}{Ra} \\ \tilde{T}_0(\eta) = -\eta \operatorname{erfc}(\alpha Ra^{1/2}\eta/2) \\ \qquad + \dfrac{2}{\alpha\sqrt{Ra\pi}}\exp(-\alpha^2 Ra\eta^2/4). \end{cases} \quad (29)$$

The dimensionless temperature at the surface of the sphere is now given by

$$T_w(t) = 2\left\{\frac{t}{\pi Ra}\right\}^{1/2}. \quad (30)$$

3. NUMERICAL TECHNIQUE

Equations (7) and (8) or (10) and (11) are now solved numerically using a standard finite-difference scheme, subject to the boundary conditions (13)–(18). Since the numerical techniques used to solve these two systems of equations are very similar to each other we will only describe that for solving equations (7) and (8).

First, if $\delta x(\delta\eta)$ and $\delta\mu$ represent the mesh size in the $x(\eta)$ and μ directions, respectively, then the constant grid lines are $x_i = i\,\delta x$ ($\eta_i = i\,\delta\eta$), $i = 0, 1, 2, \ldots M$, and $\mu_j = j\,\delta\mu$, $j = 0, 1, 2, \ldots N$, and if further we use δt to represent the increment in the t direction then $t_n = n\,\delta t$, $n = 1, 2 \ldots$. We can now represent any variable, say χ, at the point $(x, \mu, t) = (x_i, \mu_j, t_n)$ by $\chi_{i,j,n}$. If we implement the symmetrical condition for T at $\theta = \pi$, namely $\partial T/\partial\theta = 0$ at $\theta = \pi$, then we find that it is not obvious to obtain a condition on $\partial T/\partial\mu$ since at $\mu = 1 \partial T/\partial\mu = 0$ is satisfied by any finite value of T, as may be verified from equation (6). However, following Riley [10], if we expand $T = T(\theta)$ about $\theta = \pi$ then we have

$$\begin{cases} T_{i,N-1,n} = T_{i,N,n} + \frac{1}{2}(\theta_{N-1} - \pi)^2 T''_{i,N,n} + \cdots \\ T_{i,N-2,n} = T_{i,N,n} + \frac{1}{2}(\theta_{N-2} - \pi)^2 T''_{i,N,n} + \cdots \end{cases} \quad (31)$$

where the prime denotes differentiation with respect to θ, $\theta_j = 2\sin^{-1}(j\,\delta\mu)$, and we have used the fact that $T'_{i,N,n} = 0$. From equation (31) we have

$$T_{i,N-1,n} - T_{i,N,n} = \left(\frac{\theta_{N-1} - \pi}{\theta_{N-2} - \pi}\right)^2 (T_{i,N-2,n} - T_{i,N,n}). \quad (32)$$

For small values of $\theta - \pi$ it may be shown from equation (6) that $(\pi - \theta_{N-1})^2 = 1\delta\mu/2$ so equation (32) gives

$$T_{i,N,n} = 2T_{i,N-1,n} - T_{i,N-2,n} \quad (33)$$

as the symmetrical boundary condition upon T at the lower pole of the sphere.

In order to start our finite-difference calculations, the solutions which are valid for small values of t, namely expressions (22) and (29), are first calculated numerically and then the values of ψ and T at $t = \delta t$, as obtained from expressions (19) and (26), are used as the initial conditions for the constant temperature and the constant heat flux cases, respectively. From the analytic solution at $t = \delta t$, the solutions of the full equations (7) and (8) or (10) and (11) are stepped forward in time using the Crank–Nicolson scheme which is numerically stable for any size of δt and we now describe briefly the technique employed for equations (7) and (8) only, as the scheme is quite standard and equations (10) and (11) are solved in a similar manner.

Before equations (7) and (8) are solved numerically, an initial condition is required. At the initial stage, i.e. at $t = \delta t$, the numerical values of ψ and T from expression (19) are used. First we consider equation (7). This equation only contains t as a parameter and as a consequence all the derivatives are evaluated at $t = n\,\delta t$, using the central-difference scheme. This results in a set of finite-difference equations for ψ which are solved using point relaxation and in the iteration process for ψ the most updated values of ψ and T on the adjacent points to $(x, \mu) = (x_i, \mu_j)$ are used. The Crank–Nicolson scheme is used for equation (8). The derivatives of T are discretized in the usual way at both $t = (n-1)\delta t$ and $t = n\delta t$, whilst all the coefficients involved in equation (8) are evaluated at $t = (n-1/2)\delta t$ and the information at $t = \delta t$ is obtained from expression (19). Once the information at $t = (n-1)\delta t$ is obtained, the discretized form of equation (8) is solved at $t = n\delta t$. Again, the point relaxation technique is used obtain solutions for T at $t = n\delta t$; the most updated values of T and ψ around the mesh point at which $T_{i,j,n}$ are sought are used. The above iteration procedure is repeated at $t = n\delta t$ until a certain preassigned criteria for convergence is satisfied, namely, if $\psi^{(m)}$, $\psi^{(m+1)}$ and $T^{(m)}$, $T^{(m+1)}$, which are successive iterates for ψ and T at $t = n\delta t$, respectively, then we say that the numerical solution has converged when the following criteria are satisfied

$$\sum_{i,j} \{|\psi^{(m)} - \psi^{(m-1)}| + |T^{(m)} - T^{(m-1)}|\} < \varepsilon \quad (34)$$

where ε is prescribed tolerance and the summation takes place over all the mesh points. For the steady-state solution, the above procedure is carried out until t is sufficiently large that the solutions for two successive time steps are almost identical.

4. RESULTS AND DISCUSSION

Numerical results were obtained for both the constant temperature and constant heat flux cases for $0.01 \leqslant Ra \leqslant 200$, and the mesh sizes and the constant α for the calculations presented in this paper vary with Rayleigh number and are shown in Table 1.

The numerical result is found to be more sensitive to the mesh size in the x- or η-direction that to that in the μ-direction and in all the situations shown in this paper we found that any further decrease in the mesh sizes results in no significant differences in the numerical solution. The tolerance, ε, for all the calculations was chosen to be 10^{-5}, but the results found when using a smaller value did not graphically produce any difference. Instead of just performing a few time steps for solving equations (11) and (12) during the early stages of the heat conduction, we solved these equations up to $t = 1$ and then the iteration procedure was switched to equations (7) and (8).

Figure 2 shows the instantaneous streamlines for $Ra = 50$ at time $t = 1$, 3, 6, 10, 15 and 50. In each diagram, the left-hand half of each figure is for the constant temperature case, whilst the right-hand half is for the constant heat flux case. We observed that the flow field for the two cases considered are quite different from each other with, at a given value of Ra, the flow motion in the vicinity of the sphere at a given time t for the constant temperature case being much stronger than that for the constant heat flux case. In the early stages, the fluid motion is mainly confined to the vicinity of the sphere, whilst at later times, due to the convection from the sphere, the flow motion spreads outwards and upwards. From about $t = 10$, the flow pattern very close to the sphere does not change very much, as can be observed from Fig. 2(a), (e) and (f) but there is a large difference far away from the sphere, as can be seen from Fig. 2(e) and (f). The steady state may never be reached, but, after a long time, the flow near the sphere will approach a steady-state situation.

In order to demonstrate how the heat conduction develops with time, Fig. 3 shows the isothermal line $T = 0.2$ for $Ra = 1$, 5, 10, 50, 100 and 200 at time $t = 1$, 3, 6, 10 and 15 for both flow cases considered. The left-hand half of each figure is for the constant temperature cases, whilst the right-hand half is for the

Table 1. The mesh sizes and values of α

Ra	δx	$\delta\eta$	$\delta\mu$	δt	α
0.01–5	1/60	1/60	1/40	1/20	1
5–50	1/80	1/80	1/60	1/20	1.5
50	1/120	1/120	1/60	1/20	4
100	1/140	1/140	1/70	1/20	4–5
200	1/160	1/160	1/80	1/20	4–5

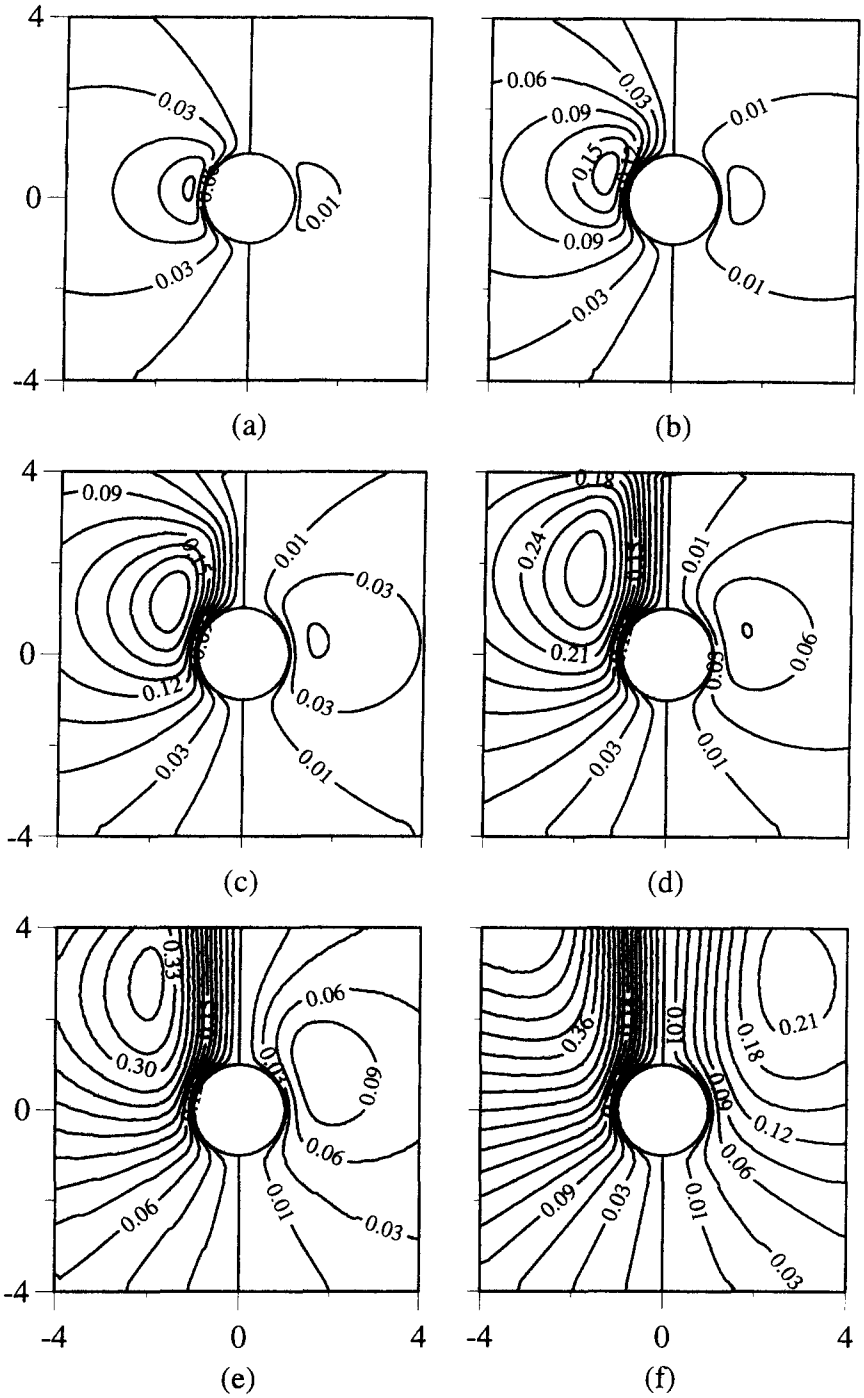

Fig. 2. The instantaneous streamlines for $Ra = 50$ at different times: (a) $t = 1$, (b) $t = 3$, (c) $t = 6$, (d) $t = 10$, (e) $t = 15$, (f) $t = 50$.

constant heat flux case. Again, we observe that the convection for the constant temperature case is stronger than that for the constant heat flux case. For relatively small values of Ra, e.g. $Ra = 1$, even at $t = 15$, the isothermal line $T = 0.2$ still looks circular, as can be seen from Fig. 3(a). As the value of Ra increases, convection starts to become more important and for $Ra \geqslant 50$ we observed a very clear cap of the plume from about $t = 10$ which travels upwards as the convection process continues. For $Ra = 1$, 5 and 10, the time at which the cap of the plume appears (for $T = 0.2$) may be greater than $t = 50$, which is the largest time for which the calculations have been performed.

For the constant temperature case, Fig. 4 shows the overall Nusselt number as a function of t for $Ra = 1$,

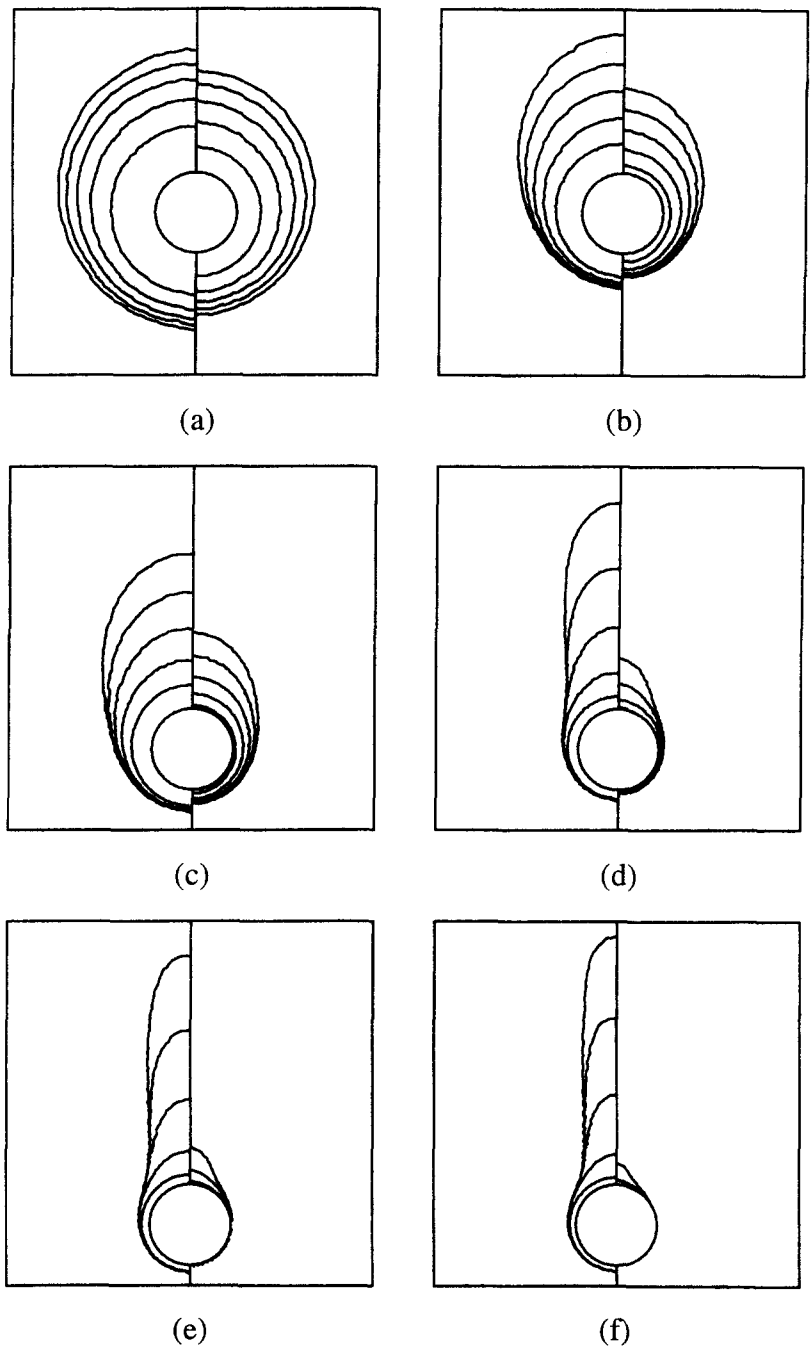

Fig. 3. The development of the isothermal line $T = 0.2$. For each diagram and the lines from the top are for $t = 15$, 10, 6, 3 and 1, respectively: (a) $Ra = 1$, (b) $Ra = 5$, (c) $Ra = 10$, (d) $Ra = 50$, (e) $Ra = 100$, (f) $Ra = 200$.

5, 10, 50, 100 and 200, together with the leading order variation of Nu for $Ra = 10$ and 50 as obtained for small values of t using expression (25). Clearly, for small values of t expression (25) gives a good approximation to the full numerical solution. It is observed that the value of the overall Nusselt number Nu settles down very quickly after $t = 5$ and this suggests that the local heat convection has reached its asymptotic 'steady state'. However, it is interesting to note that, for $Ra = 10$, 50, 100 and 200, the overall Nusselt number appears to decrease from its value at time $t = 0$ and reaches a minimum value which is below its 'steady-state' value and then it starts to increase slightly towards its 'steady-state' value. But, if the Rayleigh number is sufficiently small, the overall Nusselt number monotonically decreases towards its 'steady-state' value. It is interesting to note that in the numerical investigation of the heat transfer from a sphere for a

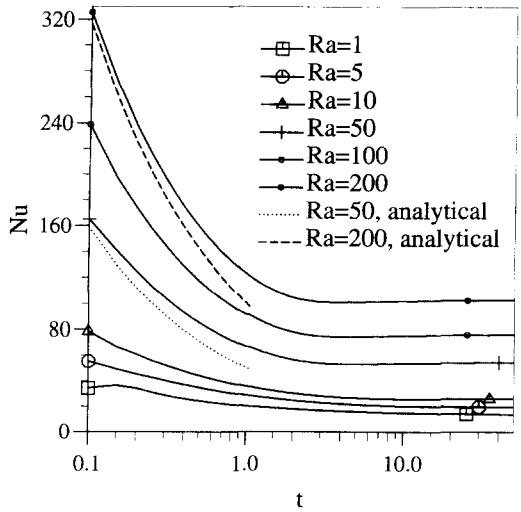

Fig. 4. Overall Nusselt number as a function of t for $Ra = 1$, 5, 10, 50, 100 and 200.

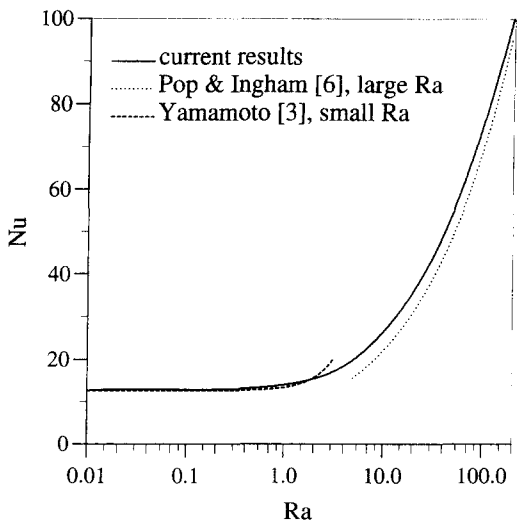

Fig. 5. Comparison of the overall Nusselt number for $t = 50$ with that of Pop and Ingham [6] and Yamamoto [3].

Newtonian flow, Riley [10] also noticed that there exists a minimum value of Nu.

In order to obtain the 'steady-state' solution, the time forward numerical procedure was carried out until the solution near the sphere at two consecutive time steps are almost identical, although as we have already mentioned, physically the real 'steady-state' may never be achieved. In all cases we considered, the value of t was found to be greater than 15 and this value depends on the value of Ra. However, for all the results presented in this paper the value of t from which the solution near the sphere is treated as being steady is taken to be 50. Figure 5 shows the overall Nusselt number at $t = 50$ as a function of Ra for the constant temperature case, together with the results obtained by Yamamoto [3] for small Ra and by Pop and Ingham [6] using a boundary-layer method where the steady-state equations were considered. We see that the results obtained in the present investigation are in very good agreement with those obtained by Pop and Ingham [6], and this agreement becomes better as Ra increases, and those of Yamamoto [3] for small values of Ra. It is interesting to note that although the result of Yamamoto [3] was initially obtained for $Ra \ll 1$, Fig. 5 shows that it is a good approximation for values of Ra up to about 2.

Figure 6 shows the temperature distribution at the upper pole of the sphere as a function of r for $Ra = 10$, 50 and 100 at different times and, as we have already noted, the convection in the constant temperature case is stronger than that in the constant heat flux case. At small values of Ra, say $Ra = 10$, see Fig. 6(a), the temperature distributions are quite smooth and the non-zero temperature field is typically confined to a region which is close to the sphere for small values of t. For larger values of Ra, it can be seen clearly that there is a front of heat travelling upwards, and beyond this the temperature is virtually zero. There are relatively large changes in both ψ and T in the front region and the number of mesh points in the that region should therefore be relatively large in order to obtain accurate solutions and that was the reason for the introduction of the parameter α. Larger values of Ra and t usually require larger values of α and smaller mesh sizes in the r-direction. The front of heat travels upwards as time increases and at the same time the temperature at this front decreases. We also noted that in the constant temperature case and for a given time, the larger the value of Ra the further the front travels in a given time. Whilst in the constant heat flux case, the larger the value of Ra the slower the front travels, as can be observed from Fig. 6; this can also be seen from Fig. 3 where the isothermal line ($T = 0.2$) is plotted for various values of Ra and t.

It should also be noted that, for a given value of Ra, as t increases, the temperature vertically above the sphere along the line $\theta = 0$ starts to oscillate. The time at which the oscillation starts varies with the value of Ra; the larger the value of Ra, the earlier the oscillation starts. For $Ra = 100$, this oscillation starts at about $t = 10$ in the constant temperature case, as can be seen from Fig. 6(c). It is also observed that once this oscillation starts it always occurs at later times. The oscillation starts at a later time in the constant heat flux case than that in the constant temperature case since the convection in this case is much weaker, as we have already mentioned, and for $Ra = 100$ there is still no oscillation at $t = 50$, as can be seen from Fig. 6(c). We believe that this oscillation phenomenon is probably due to a physical instability of the problem and further investigations are required to clarify this. It is also interesting to note that in a similar investigation of the free convection Newtonian flow from

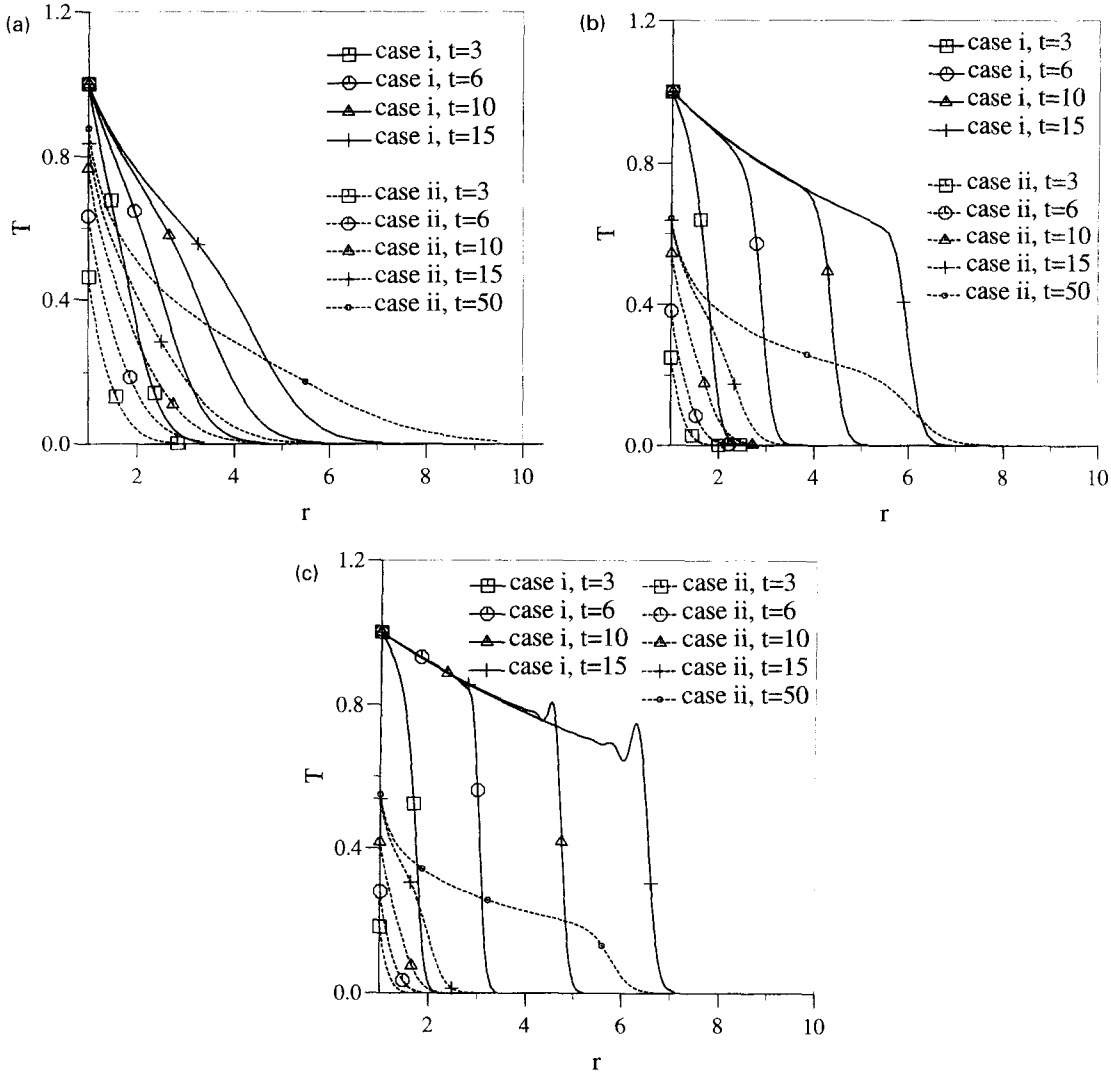

Fig. 6. The temperature distribution as a function of r at the upper pole at different times: (a) $Ra = 10$, (b) $Ra = 50$, (c) $Ra = 100$.

a sphere by Riley [10], oscillations in temperature vertically above the sphere along $\theta = 0$ are also reported for large values of t.

Figure 7 shows the variation of temperature on the surface of the sphere as a function of θ at different time for $Ra = 10$, 50 and 100 for the constant heat flux case. The first thing we observed is that the maximum and minimum temperature is always at the top ($\theta = 0$) and bottom ($\theta = \pi$), respectively. Further, it is seen that the temperature for small values of Ra settles down much more slowly than that for large values of Ra with the temperature reaching its asymptotic value at about $t = 25$ for $Ra = 10$, at about $t = 15$ for $Ra = 50$, and for $Ra = 50$ and 100 the temperature profile at $t = 50$ is almost identical to that at $t = 15$. It is also interesting to note that the 'steady-state' temperature for small values of Ra is higher than that for larger values of Ra.

Figure 8 shows the temperature, T_w, at both the lower pole ($(r, \theta) = (1, \pi)$) and the upper pole ($(r, \theta) = (1, 0)$) of the sphere as a function of Ra at time $t = 50$, which is sufficiently large for the flow near to the sphere to be considered as being in 'steady-state'. It is clear that T_w decreases as the value of Ra increases, as we have already seen from Fig. 7. This is expected since for large values of Ra the convection is strong, and as a result more heat is convected away from the sphere, and the temperature on the surface is, therefore, lower than that for small values of Ra. The larger the value of Ra the lower the surface temperature and one can vary the value of Ra, or the heat flux, in order to obtain a desired surface temperature. The temperature difference between the upper and lower poles is very small for small values of Ra but as the value of Ra increases, convection becomes more important and as a result this difference becomes

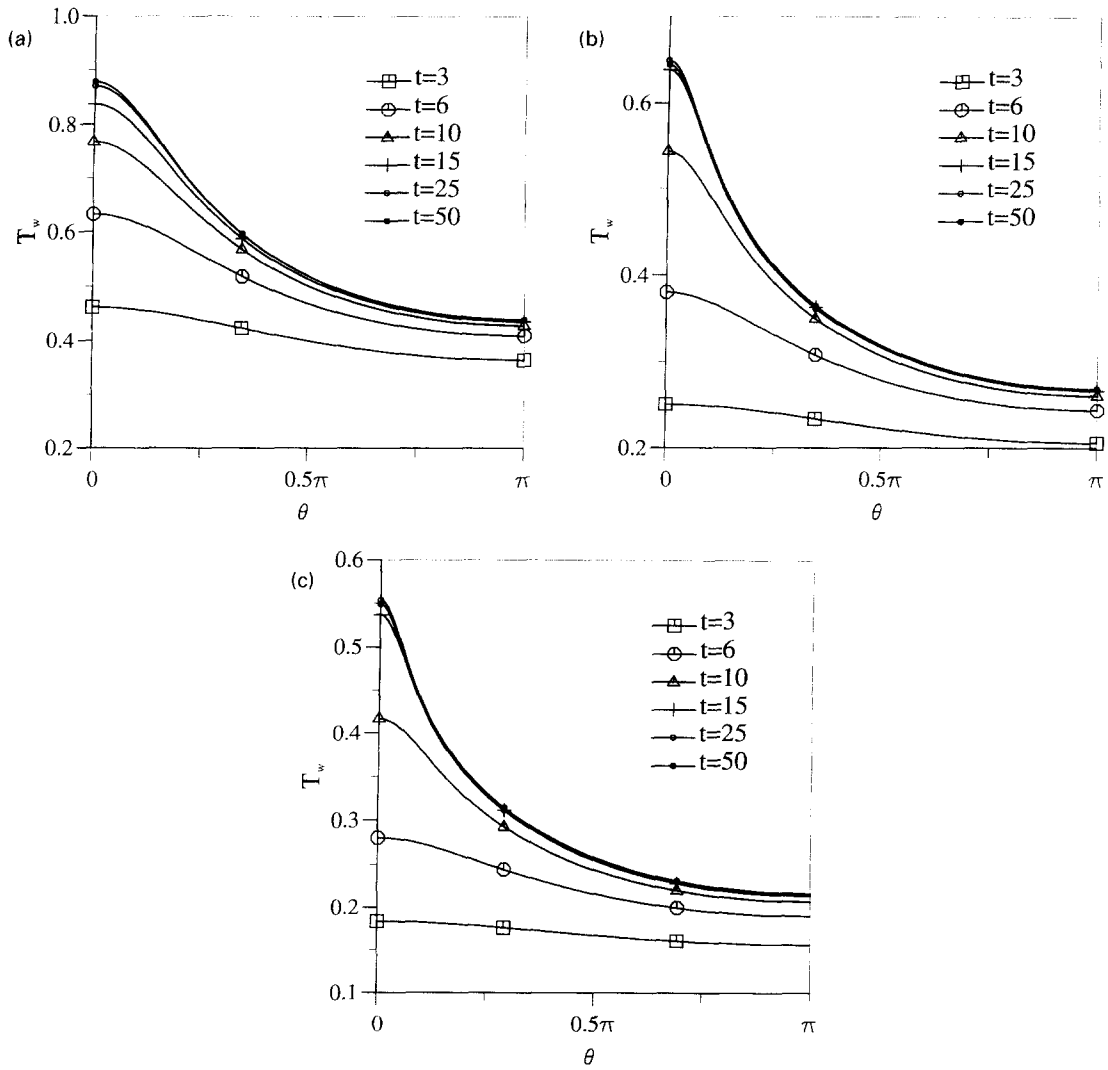

Fig. 7. Variations of the temperature on the surface of the sphere as a function of θ in the constant heat flux case: (a) $Ra = 10$, (b) $Ra = 50$, (c) $Ra = 100$.

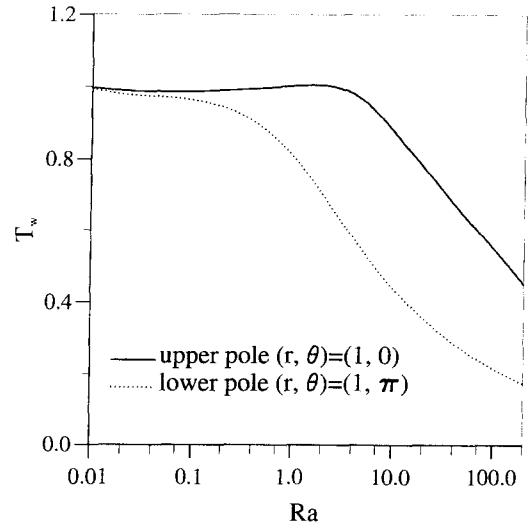

Fig. 8. The surface temperature as a function of Ra at the upper and lower poles of the sphere for $t = 50$.

larger. This difference in temperatures then does not vary much for $Ra > 0(1)$.

In order to see details of the temperature distribution at large times, Fig. 9 shows the steady isothermal lines, or more precisely those at $t = 50$, for $Ra = 50$ in the vicinity of the sphere for both the constant temperature and constant heat flux cases. It is observed from the constant temperature situation that even at $t = 50$ the front of the heat is still very strong. The small bulge behind the front represents the oscillation phenomenon mentioned earlier and oscillation starts at about $t = 25$. In the constant heat flux case, the heat is confined in a much smaller region than that in the constant temperature case and no oscillations in temperature are detected up to a time $t = 50$.

Acknowledgements—B. Yan wishes to thank the University of Cluj for their hospitality and generosity during his visit. The authors wish to thank Professor N. Riley for some very helpful discussions.

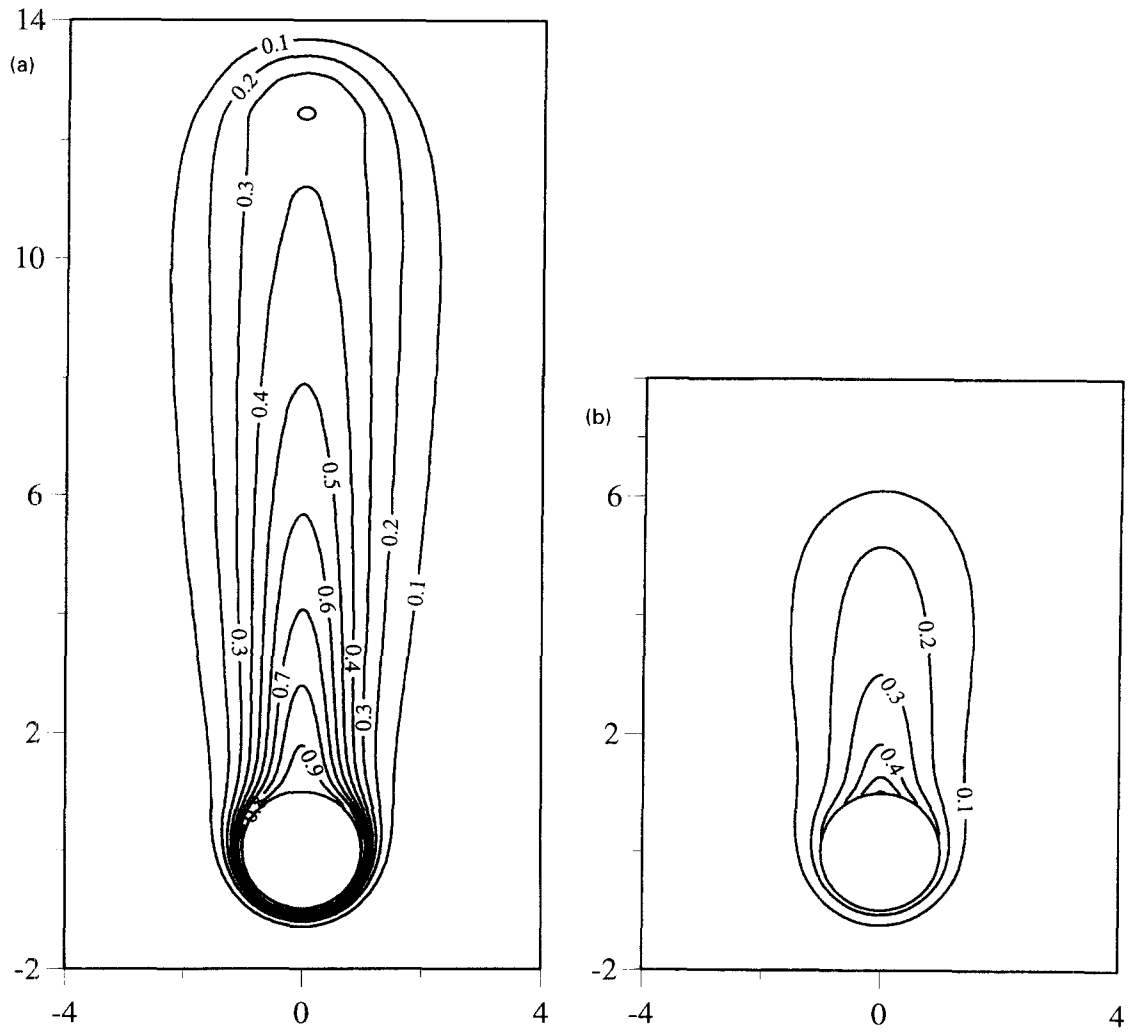

Fig. 9. The isotherms for $Ra = 50$ at $t = 50$: (a) constant temperature case, (b) constant heat flux case.

REFERENCES

1. D. A. Nield and A. Bejan, *Convection in Porous Media*. Springer, New York, 1992.
2. A. Nakayama, *PC-Aided Numerical Heat Transfer and Convective Flow*. CRC Press, Tokyo, 1995.
3. K. Yamamoto, Natural convection about a heated sphere in a porous medium. *Journal of the Physics Society of Japan*, 1974, **37,** 1164–1166.
4. J. H. Merkin, Free convection boundary layers on axisymmetric and two-dimensional bodies of arbitrary shape in saturated porous medium. *International Journal of Heat and Mass Transfer*, 1979, **22,** 1461–1462.
5. A. Nakayama and H. Koyama, Free convection heat transfer over a nonisothermal body of arbitrary shape embedded in a fluid-saturated porous medium. *Journal of Heat Transfer*, 1987, **109,** 125–130.
6. I. Pop and D. B. Ingham, Natural convection about a heated sphere in a porous medium, *Proceedings of the Ninth International Heat Transfer Conference*, 1990, Vol. 2, pp. 567–572.
7. T. Sano and R. Okihara, Natural convection around a sphere immersed in a porous medium at small Rayleigh numbers. *Fluid Dynamics Research*, 1994, **13,** 39–44.
8. H. D. Nguyen and S. Paik, Unsteady mixed convection from a sphere in water-saturated porous medium with variable surface temperature/heat flux. *International Journal of Heat and Mass Transfer*, 1994, **37,** 1783–1793.
9. T. Miloh and P. A. Tyvand, Transient free convection from a sphere embedded in a porous medium (in preparation).
10. N. Riley, The heat transfer from a sphere in free convective flow. *Computers & Fluids*, 1986, **14,** 225–237.